

# A Label Propagation Strategy for CutMix in Multi-Label Remote Sensing Image Classification

Tom Burgert, *Member, IEEE*, Kai Norman Clasen, *Member, IEEE*, Jonas Klotz, *Member, IEEE*, Tim Siebert, *Member, IEEE*, and Begüm Demir, *Senior Member, IEEE*

**Abstract**—The development of supervised deep learning-based methods for multi-label scene classification (MLC) is one of the prominent research directions in remote sensing (RS). Yet, collecting annotations for large RS image archives is time-consuming and costly. To address this issue, several data augmentation methods have been introduced in RS. Among others, the data augmentation technique CutMix, which combines parts of two existing training images to generate an augmented image, stands out as a particularly effective approach. However, the direct application of CutMix in RS MLC can lead to the erasure or addition of class labels (i.e., label noise) in the augmented (i.e., combined) training image. To address this problem, we introduce a label propagation (LP) strategy that allows the effective application of CutMix in the context of MLC problems in RS without being affected by label noise. To this end, our proposed LP strategy exploits pixel-level class positional information to update the multi-label of the augmented training image. We propose to access such class positional information from reference maps associated to each training image (e.g., thematic products) or from class explanation masks provided by an explanation method if no reference maps are available. Similarly to pairing two training images, our LP strategy carries out a pairing operation on the associated pixel-level class positional information to derive the updated multi-label for the augmented image. Experimental results show the effectiveness of our LP strategy in general and its robustness in the case of various simulated and real scenarios with noisy class positional information in particular.

**Index Terms**—CutMix, data augmentation, label propagation strategy, multi-label scene classification (MLC), remote sensing (RS)

## I. INTRODUCTION

THE growing interest in Earth observation has led to significant technological advancements, contributing to a recent surge in the availability of remote sensing (RS) image archives. Typically, an RS image scene consists of multiple classes and, thus, can simultaneously be associated with different land use land cover (LULC) class labels (i.e., multi-labels). Therefore, the development of multi-label scene classification (MLC) methods that aim to automatically assign multiple labels to each image in an archive attracts growing research interest in the RS community [1], [2], [3]. In particular, MLC gains popularity due to its capacity of facilitating a quick categorization and understanding of the image scenes. Aligned with the advances in machine learning, deep neural networks

play a crucial role for many state-of-the-art results in RS MLC. As a result of costly and time-consuming annotation processes, an important factor to improve the generalization performance of these networks is the use of data augmentation techniques. Data augmentation refers to the process of creating slightly modified versions of existing training images by applying stochastic transformations to the images that preserve their semantic characteristics. Consequently, deep neural networks trained with augmented images are less prone to overfit on individual images and, simultaneously, gain a diversified understanding of individual classes as the effective amount of training images is increased. The data augmentation techniques proposed in the literature typically function in a task-agnostic manner. Most of the existing techniques are initially presented in the context of single-label image classification (assigning a single high-level category label to each image), but are also applied in other related image recognition tasks such as MLC, object detection, or semantic segmentation (i.e., pixel-based classification). While a wide range of data augmentation techniques can also be directly applicable to RS MLC, its current utilization is limited to simple techniques like image rotations, translations, and flipping [4].

Among different data augmentation techniques, CutMix [5] stands out as a particularly effective approach. It is inspired by the success of the box augmentation strategy CutOut [6], [7] that removes areas from an image and replaces them with zeros or random noise to enhance model robustness against partially invisible class features (e.g., occlusion, cut-off parts). CutMix takes this concept further by filling informative parts from different images into the uninformative cutout areas and updating the label accordingly. Consequently, CutMix not only ensures model robustness to partially invisible class features but also introduces an additional learning signal, enriching the model's understanding of the data. Due to its effectiveness, CutMix has been successfully adopted for RS tasks, such as single-label scene classification [8], ship object detection [9], and semantic segmentation [10].

However, in contrast to simple image transformations that preserve the whole training image (e.g., rotation, flipping), the use of CutMix for MLC problems remains challenging. Unlike object detection and semantic segmentation, there is no direct access to pixel-level class positional information in MLC to correctly update the multi-labels. Applying CutMix to multi-label images without a proper label update strategy can result in the introduction of multi-label noise [11]. If a class is only present in the cutout area, the application of CutMix can lead

T. Burgert, K. N. Clasen, J. Klotz, T. Siebert, and B. Demir are with the Berlin Institute for the Foundations of Learning and Data (BIFOLD) and with the Faculty of Electrical Engineering and Computer Science, Technische Universität Berlin, 10623 Berlin, Germany (emails: t.burgert@tu-berlin.de, k.clasen@tu-berlin.de, j.klotz@tu-berlin.de, siebert@tu-berlin.de, demir@tu-berlin.de). Except for the first and the last author, the order was determined alphabetically.

to additive noise, as the multi-label would incorrectly indicate the presence of this class. On the other hand, if a new class is contained in the pasted area originating from a different image, the application of CutMix can lead to subtractive noise as the multi-label would incorrectly indicate the absence of the class.

To overcome the problem of introducing multi-label noise when directly applying CutMix in RS MLC, we propose a label propagation (LP) strategy that enables the correct update of the multi-label of a CutMix-augmented image. In addition to pairing two images, the LP strategy carries out a pairing operation on associated pixel-level class positional information to derive the updated multi-label vector for the augmented image. In detail, we consider two scenarios associated to the availability of pixel-level class positional information. In the first scenario, we assume that the multi-labels of the images originate from associated reference maps (i.e., each class label annotated in the reference map is indicated as present in the multi-label). In other words, for each training image class labels are not only available at image-level but also at pixel-level. These reference maps may comprise different levels of unreliability depending on the considered way of obtaining the map. In the case that the associated reference maps are obtained via manual annotation of each pixel (e.g., DeepGlobe dataset [12]), unreliability in class positional information can arise from labeling errors in the manual pixel annotation of the images. In the case that the associated reference maps are obtained through the inference of a segmentation model (i.e., pixel-based classification model) (e.g., Dynamic World dataset [13]), unreliability in class positional information can originate from inaccurate predictions. In the case that the associated reference maps are obtained from thematic products [14], [15], [16], [17] (e.g., BigEarthNet [18]), unreliability in class positional information can have various causes, such as (i) different resolutions between thematic product and the considered image, (ii) imprecise co-registration of thematic product and the considered image, (iii) temporal difference between thematic product and the considered image, or (iv) labeling error in the thematic product. In the second scenario, we assume that associated reference maps are not available. Thus, each training image is only annotated with image-level multi-labels. In this case, we propose to leverage post hoc explanation methods to create class explanation masks that attribute each class that is indicated as present in the multi-label of an image with the respective relevant pixels. Likewise, the second scenario may also include unreliability due to imprecise explanations. Experimental results obtained on three diverse datasets show the effectiveness of our LP strategy in general and robustness to not fully reliable (i.e., noisy) pixel-level class positional information in particular.

In summary, our contributions are the following:

- We propose an LP strategy that allows the effective application of CutMix to RS MLC without being affected by multi-label noise.
- To the best of our knowledge, we are the first to explore the benefits of thematic products and explanation methods to provide pixel-level class positional information for

correctly updating the multi-labels of a CutMix-augmented image in RS MLC.

- We conduct extensive experiments considering class positional information with varying levels of reliability. In particular, we show the effectiveness of our LP strategy for: (i) reliable class positional information; (ii) a variety of six simulated types of noisy class positional information; (iii) a scenario in which the noisy class positional information is provided by thematic products; and (iv) a scenario in which the noisy class positional information is provided by explanation methods.

The rest of the paper is organized as follows. Section II surveys the related data augmentation techniques presented in computer vision (CV) and RS communities. In Section III, our LP strategy that allows the application of CutMix in the framework of MLC problems in RS is introduced. Section IV describes the considered multi-label datasets and the experimental setup, while the experimental results are presented in Section V. Finally, in Section VI, the conclusion of the work is drawn.

## II. RELATED WORK

According to our knowledge, there is no data augmentation techniques specifically designed and developed for MLC problems. Most of the existing data augmentation techniques are considered to be task-agnostic, and thus, directly used in MLC problems. Therefore, in this section, we provide a general overview of data augmentation techniques developed for different image recognition tasks in the CV and RS communities.

In detail, data augmentation techniques play a crucial role for state-of-the-art results in supervised [19], [20], [21], semi-supervised [22], [23], [24], and self-supervised learning [25], [26], [27] in CV. Notably, these techniques demonstrate their effectiveness in single-label classification (SLC) but also in related tasks like object detection [28], and semantic segmentation [29]. Similarly to CV, data augmentation techniques significantly improve the performance and generalization capabilities for RS tasks. Recently, researchers have explored various approaches to tailor well-established CV data augmentation techniques for RS tasks, such as SLC [8], [30], [31], [32], [33], object detection [9], [34], [35], [36], [37], [38], or semantic segmentation tasks [10], [39]. Joined in their purpose to alleviate overfitting and to serve as a form of regularization in small data regimes, the approaches for data augmentation can be broadly divided into three categories: (i) image modification (Section II-A); (ii) image generation (Section II-B); or (iii) image pairing (Section II-C) that also includes CutMix-based approaches.

### A. Image Modification based Data Augmentation

The earliest data augmentation techniques developed are based on image modifications [40]. These techniques aim to encode invariances to data distortions. Image modifications can be grouped into two variants: (i) geometric transformations and (ii) channel transformations. Geometric transformations involve operations like horizontal flips, random crops, pixel shifts,

distortions to orientations, or random erasing (i.e., CutOut) [6], [7]. Conversely, channel transformations include operations like color distortions, contrast and brightness adjustments, or histogram equalization. Both types of transformations are applied successfully to standard CV benchmarks such as CIFAR [41] and ImageNet [42] (e.g., [43], [44], [45]).

Many of these image modification techniques, in particular geometric transformations, also belong to the standard training repertoire for various RS benchmarks [46], [47], [48]. In addition, Ding et al. [30] find augmentations of translation, pose synthesis, and speckle noise to be beneficial for the task of vehicle classification on synthetic aperture radar (SAR) data. Wei Zhang and Yungang Cao [33] address the differences of object structures in RS SLC in comparison to CV SLC (e.g., smaller objects, less connected objects, less central objects) by utilizing class activation maps (CAMs) [49]. CAMs are used to constrain the geometric transformations of cropping and translation by guaranteeing a minimum area of the relevant pixels to be retained. Further, Gaussian noise injection is constrained by weighting it by the inverse of the contribution of pixels to the final prediction.

### B. Image Generation based Data Augmentation

In the context of image generation, various data augmentation techniques are proposed to enhance generalization performance by leveraging synthetically generated images. These approaches have in common that they employ a generative adversarial network (GAN) for image generation. In particular, GAN-based data augmentation techniques show beneficial effects under scarce data regimes [50], [51] or for few-shot learning tasks [52]. Additionally, Geirhos et al. [53] improve the robustness of neural networks towards adversarial examples with a GAN-based ImageNet stylizing approach that guides the network to prioritize shape over texture.

In RS, image generation approaches are mainly proposed for object detection tasks focused on vehicles like aircraft, ships, or ground vehicles, in which images are commonly rare and costly to annotate. While Yan et al. create new images by integrating existing 3D models of different ships [34] or aircraft [54] into real RS scenes, Zheng et al. [35] synthesize realistic ground vehicles by making use of a GAN. Furthermore, Xiao et al. [32] extend the integration of 3D models of ships by applying a neural style transfer (NST) network termed Sim2RealNet to eliminate the domain gap between real and simulated images for single-label ship classification.

### C. Image Pairing based Data Augmentation

Data augmentation techniques aligned with the third category involve mixing existing images with appropriate changes to ground reference labels. Mixup [55] most prominently creates convex combinations of pairs of images and their corresponding labels, favoring simple linear behavior in between training images. Until now, Mixup still forms the basis of many state-of-the-art approaches in semi-supervised [23] and label noise robust learning [56]. Inspired by the image pairing approach of Mixup, CutMix extends the box augmentation technique

of random erasing (i.e., CutOut) by pasting corresponding bounding boxes of other training images into the erased areas. Further extensions of CutMix exist that paste multiple boxes based on the most attentive regions [57]. The equivalent for CutMix in object detection consists of copying object instances (i.e., bounding boxes) and paste-blending them onto diverse backgrounds [58]. On the other hand, in semantic segmentation, CutMix-inspired approaches commonly termed as copy-paste mechanisms operate at pixel-level [29]. Moreover, in object detection, Mosaic augmentation further extends CutMix by stitching four resized images together, followed by a random crop that retains parts of every image.

Likewise, the majority of adoptions of image pairing approaches in RS is based on the concepts of the image blending technique Mixup [55], or the box augmentation technique CutMix [5]. In SLC, Lu et al. [8] propose RSI-Mix, a variant of CutMix that selects two images of the same category and copy-pastes a selected bounding box from one image to another. Moreover, Yan et al. [31] beneficially integrate Mixup into a semi-supervised framework for SLC. In object detection, Suo et al. [9] elaborate CutMix for artificially increasing the object density by pasting existing bounding box annotations of ships from different images onto a single target image. Zhao et al. [37] introduce a variant of the Mosaic data augmentation technique that puts special emphasis on rare or hard-to-detect class objects and tackles the problem of class imbalances via a joint data augmentation technique that makes use of Mixup, Mosaic, and SMOTE [59]. Further, Zhang et al. [36] propose Object First Mixup, an alteration to Mixup that adjusts the weights of segmented objects and their background in semi-supervised object detection. Finally, in semantic segmentation, You et al. [39] incorporate the copy-paste mechanism (which is the pixel annotation-based equivalent of CutMix) into a semi-supervised framework in which the ground reference pixels of annotated roads are pasted onto unlabeled images. Concurrently, the framework RanPaste introduced by Wang et al. [10] exploits color jitter and random Gaussian noise for consistency regularization while making use of a CutMix-like pasting mechanism that pastes a bounding box (in contrast to pixels of a segment) of a labeled image onto an unlabeled image. Consequently, a pseudo-label mask for the paired image is inferred from the predictions of a student model.

In contrast to image modification and image generation approaches as well as Mixup, the application of CutMix in MLC tasks can lead to the erasure or addition of class labels in the augmented (i.e., paired) image. To address this problem, we propose an LP strategy that enables the correct update of the multi-label of the augmented image for RS MLC.

## III. PROPOSED STRATEGY

In this section we introduce our label propagation (LP) strategy that aims to allow an effective application of CutMix for MLC problems in RS. Let  $\mathcal{D} := \{(\mathbf{x}_1, \mathbf{y}_1), \dots, (\mathbf{x}_N, \mathbf{y}_N)\}$  be a multi-label training set, where  $N \in \mathbb{N}$  is the number of training images. Each pair  $(\mathbf{x}_i, \mathbf{y}_i)$  in  $\mathcal{D}$  consists of an image  $\mathbf{x}_i \in \mathbb{R}^{C \times H \times W}$ , where  $C$  is the number of image

bands with a height  $H$  and a width  $W$ , and its multi-label vector  $\mathbf{y}_i \in \{0, 1\}^L$ , where  $L \in \mathbb{N}$  defines the number of classes. Each entry  $(\mathbf{y}_i)_l$  relates to the presence (i.e., 1) or absence (i.e., 0) of the respective class  $l$ . We aim to train a deep neural network  $h$  such that it generalizes well to classify unseen images correctly. We assume that  $|D|$  is not sufficiently large and that the data annotation process is costly and time-consuming. To overcome this issue, we adopt the CutMix algorithm due to its proven success into our training procedure for improving the performance of  $h$ . However, as mentioned before, the labels in MLC do not explicitly indicate class positional information. Therefore, applying CutMix to training images annotated with multi-labels can lead to the potential erasure or addition of class labels in the paired image and, thus, may lead to multi-label noise. To address this problem, we propose an LP strategy that aims to preserve the correct class information within the multi-label vector of the augmented image to enable an effective application of CutMix in MLC. In detail, for accessing pixel-level class positional information that is incorporated by our LP strategy into the CutMix process, we consider two scenarios: (i) the usage of reference maps that correspond to the multi-labels, or (ii) the usage of class explanation masks provided by explanation methods if no reference maps are available. In the following, we initially define the algorithm for CutMix in MLC. Thereafter, our LP strategy for CutMix in MLC is introduced for both scenarios. Finally, the section is concluded by a specification of the box creation algorithm as well as the application procedure of CutMix with our LP strategy to an MLC task.

#### A. Definition of the CutMix Algorithm

Let a box (i.e., rectangular region)  $R = (r_a, r_b, r_c, r_d)$  be specified through the left lower corner  $(r_a, r_b)$  and the right upper corner  $(r_c, r_d)$ , respectively. Then, the area of the box is denoted as  $A_R = (r_c - r_a)(r_d - r_b)$ . Further, the binary mask  $B_R = (b_{j_1 j_2})_{j_1 j_2} \in \mathbb{R}^{H \times W}$  corresponding to a box  $R$  is defined, where  $b_{j_1 j_2}$  is defined for  $j_1, j_2 = 1, \dots, n$  as follows:

$$b_{j_1 j_2} = \begin{cases} 1, & \text{if } r_a \leq j_1 \leq r_c \text{ and } r_b \leq j_2 \leq r_d \\ 0, & \text{otherwise.} \end{cases} \quad (1)$$

The goal of CutMix is to generate an augmented training image  $\tilde{\mathbf{x}}$  with a corresponding multi-label vector  $\tilde{\mathbf{y}}$  by combining two existing training images  $\mathbf{x}_1, \mathbf{x}_2$  and its corresponding label vectors  $\mathbf{y}_1, \mathbf{y}_2$ . Therefore, the two boxes  $R_1$  and  $R_2$ , and their corresponding binary masks  $B_1$  and  $B_2$  are generated. To erase  $R_1$  from  $\mathbf{x}_1$ , the inverse binary mask  $(1 - B_1)$  is combined with  $\mathbf{x}_1$  through the Hadamard product, as  $(1 - B_1) \odot \mathbf{x}_1$ . Further, the box  $R_2$  is extracted from  $\mathbf{x}_2$  by applying the Hadamard product between  $\mathbf{x}_2$  and the binary mask  $B_2$ , as  $B_2 \odot \mathbf{x}_2$ . To fill the erased area in  $\mathbf{x}_1$  with the box selected from  $\mathbf{x}_2$ , the two boxes have to be spatially aligned. This alignment is carried out by the image shift operator  $T_{R_2 R_1}^x : \mathbb{R}^{C \times H \times W} \rightarrow \mathbb{R}^{C \times H \times W}$ . To explain in detail the working principle of the image shift operator for a single image band (i.e., when  $C = 1$ ), let us

assume that the unaligned matrices  $B_1 \odot \mathbf{x}_1$  and  $B_2 \odot \mathbf{x}_2$  have the following block matrix structures:

$$B_1 \odot \mathbf{x}_1 = \begin{pmatrix} 0 & 0 \\ 0 & \mathbf{x}_{R_1} \end{pmatrix} \quad (2)$$

$$B_2 \odot \mathbf{x}_2 = \begin{pmatrix} \mathbf{x}_{R_2} & 0 \\ 0 & 0 \end{pmatrix}. \quad (3)$$

Then,  $T_{R_2 R_1}^x$  shifts  $\mathbf{x}_{R_2}$  to the position of  $\mathbf{x}_{R_1}$  as:

$$T_{R_2 R_1}^x(B_2 \odot \mathbf{x}_2) = \begin{pmatrix} 0 & 0 \\ 0 & \mathbf{x}_{R_2} \end{pmatrix}. \quad (4)$$

This shift can be represented by (channel-wise) matrix multiplication with block-identity matrices. To generate the corresponding multi-label vector  $\tilde{\mathbf{y}}$ ,  $\mathbf{y}_1$  and  $\mathbf{y}_2$  are weighted by the respective remaining sizes of the paired image parts of  $\mathbf{x}_1$  and  $\mathbf{x}_2$ . Then, the augmented pair  $(\tilde{\mathbf{x}}, \tilde{\mathbf{y}})$  is defined by the two pairing operations:

$$\tilde{\mathbf{x}} = (1 - B_1) \odot \mathbf{x}_1 + T_{R_2 R_1}^x(B_2 \odot \mathbf{x}_2) \quad (5)$$

$$\tilde{\mathbf{y}} = (1 - A_R)\mathbf{y}_1 + A_R\mathbf{y}_2. \quad (6)$$

It is worth noting that there exist multiple versions of CutMix. In this work, CutMix with unaligned positions of the boxes  $R_1$  and  $R_2$  is considered to increase the diversity of the augmented images. For further details, we refer the reader to the original CutMix paper [5].

#### B. Proposed Label Propagation Strategy for CutMix in Multi-Label Remote Sensing Image Classification

The proposed LP strategy aims to preserve all class labels in the augmented image by leveraging pixel-level class positional information. In detail, we consider two scenarios in which each training image is associated with such class positional information. In the first scenario, the training images are associated with reference maps that directly correspond to the multi-label of the image. In the second scenario, the training images are associated with class explanation masks that are obtained by an explanation method if no reference maps are available. Analogously to the application of the pairing operation for two images in (5), our LP strategy additionally applies this operation to the pixel-level class positional information of the two images and derives the multi-label vector from the paired information. In the following, the variants of our LP strategy for the respective two scenarios to effectively apply CutMix in MLC are described.

##### Scenario 1: Label Propagation based on Reference Maps

In the first scenario, we assume the existence of associated reference maps. Following the general notation of  $[k_1, k_2]_{\mathbb{N}} := \{j \in \mathbb{N} \mid k_1 \leq j \leq k_2\}$  for  $k_1, k_2 \in \mathbb{N}$ , for each of the pairs  $(\mathbf{x}_i, \mathbf{y}_i)$  in  $D$ , let  $\mathbf{m}_i \in [0, L]_{\mathbb{N}}^{H \times W}$  be a pixel-level reference map associated with the image  $\mathbf{x}_i$ , where each entry in  $\mathbf{m}_i$  indicates the class label of one of the classes present in  $\mathbf{y}_i$ . In this scenario, we apply a pairing operation analogous to



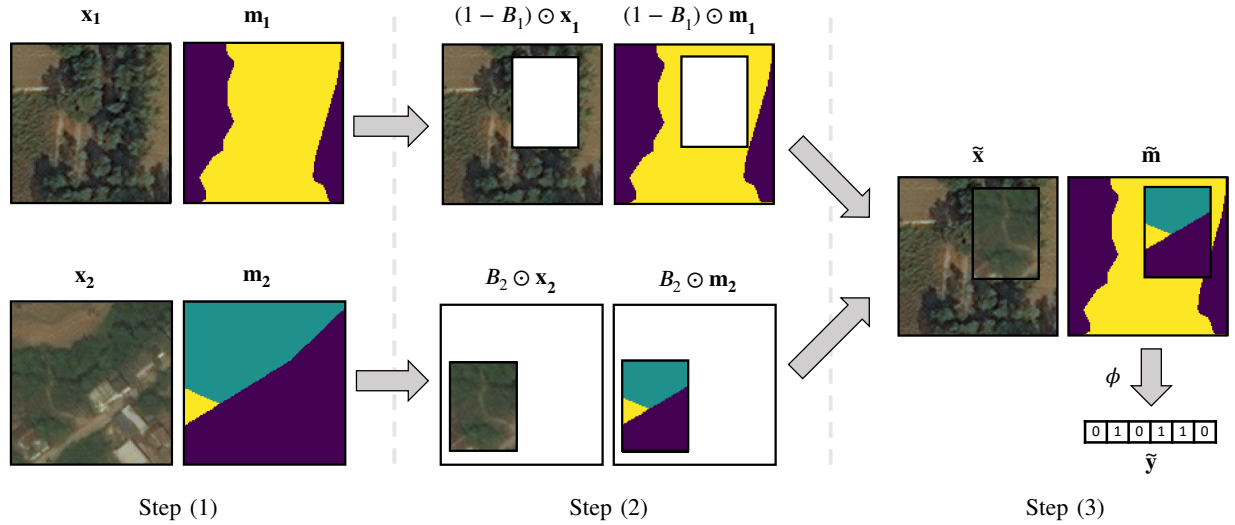


Figure 1: Schematic illustration of the LP strategy for CutMix in MLC leveraging reference maps. Step (1): the training images and associated reference maps  $(x_1, m_1)$ ,  $(x_2, m_2)$  are selected. Step (2): the binary mask  $B_1$  erases a box from  $(x_1, m_1)$ , and the binary mask  $B_2$  extracts a box of the same size from  $(x_2, m_2)$ , respectively. Step (3): the augmented training image  $\tilde{x}$  and reference map  $\tilde{m}$  are created by leveraging the shift operators to replace the erased area of  $(x_1, m_1)$  with the extracted box from  $(x_2, m_2)$ . The reference map  $\tilde{m}$  is then used to derive the updated multi-label vector  $\tilde{y}$  for  $\tilde{x}$  through the function  $\phi$ .

the pairing of  $x_1, x_2$  for the two reference maps  $m_1, m_2$ . Therefore, we define the reference map shift operator  $T_{R_2 R_1}^m : [0, L]_{\mathbb{N}}^{H \times W} \rightarrow [0, L]_{\mathbb{N}}^{H \times W}$ . Further, a read-out function  $\phi : [0, L]_{\mathbb{N}}^{H \times W} \rightarrow \{0, 1\}^L$  is defined to extract the class positional information of the updated reference map  $\tilde{m}$  to generate  $\tilde{y}$ . In particular,  $\phi$  returns the set over all entries (class labels) of the reference map  $\tilde{m}$ . Therefore, integrating the LP strategy for CutMix yields the augmented pair  $(\tilde{x}, \tilde{y})$ , where

$$\tilde{x} = (1 - B_1) \odot x_1 + T_{R_2 R_1}^x(B_2 \odot x_2) \quad (7)$$

$$\tilde{m} = (1 - B_1) \odot m_1 + T_{R_2 R_1}^m(B_2 \odot m_2) \quad (8)$$

$$\tilde{y} = \phi(\tilde{m}). \quad (9)$$

An illustration of the proposed LP strategy that allows the application of CutMix in multi-label classification problems can be found in Figure 1. First, two training images  $x_1, x_2$  with their associated reference maps  $m_1, m_2$  are selected (Step 1). Then, analogously to CutMix in SLC, two boxes  $R_1$  and  $R_2$  and their corresponding binary masks  $B_1$  and  $B_2$  are generated to extract boxes from  $(x_2, m_2)$  and erase the inverse counterpart boxes from  $(x_1, m_1)$  (Step 2). The pairing of the masked images and reference maps is carried out by the shift operators  $T_{R_2 R_1}^x$  and  $T_{R_2 R_1}^m$ . Finally, the multi-label vector  $\tilde{y}$  is read-out by  $\phi$  from the updated reference map  $\tilde{m}$  to yield the augmented pair  $(\tilde{x}, \tilde{y})$  (Step 3).

#### Scenario 2: Label Propagation based on Class Explanation Masks

In the second scenario, we assume that there is no associated reference maps available. To address this issue, we propose to use explanation methods to provide the source for pixel-level class positional information that can be leveraged by our LP strategy. Let each of the pairs  $(x_i, y_i)$  in  $D$  be associated with a set of class explanation masks  $e_i \in \{0, 1\}^{L \times H \times W}$  generated by

an explanation method. An entry of one in  $(e_i)_l \in \{0, 1\}^{H \times W}$  corresponds to a pixel (i.e., activating pixel) in the image that is attributed importance for predicting class  $l$ . To enable the pairing operation for two sets of class explanation masks  $e_1, e_2$ , we define the class explanation mask shift operator  $T_{R_2 R_1}^e : \{0, 1\}^{L \times H \times W} \rightarrow \{0, 1\}^{L \times H \times W}$ . Further, a read-out function  $\psi : \{0, 1\}^{L \times H \times W} \rightarrow \{0, 1\}^L$  is defined to derive  $\tilde{y}$  from the updated class explanation mask  $\tilde{e}$ . To address the higher uncertainty between activating and non-activating pixels in border regions of the class explanation masks, this function returns a class  $l$  as present in the updated multi-label vector  $\tilde{y}$  if the total number of activating pixels is greater than a minimum pixel threshold  $t_{\text{map}}$ . Note that if a class does not belong to the actual multi-label of the corresponding image, the whole explanation mask of this class is set to zero. Thus, it is ensured to only derive reasonable classes in the updated multi-label vector  $\tilde{y}$ . Consequently, when leveraging class explanation masks, the augmentation procedure to generate  $\tilde{x}$  is equivalent to (7), while the notation to derive  $\tilde{y}$  from a set of updated class explanation mask  $\tilde{e}$  is similar to (8) and (9), as

$$\tilde{e} = (1 - B_1) \odot e_1 + T_{R_2 R_1}^e(B_2 \odot e_2) \quad (10)$$

$$\tilde{y} = \psi(\tilde{e}). \quad (11)$$

It is worth noting that the class explanation masks can be provided by any explanation method. While some explanation methods directly output class explanations in the form of binary masks, other methods only provide class explanation heatmaps, where each pixel is associated with a probability of contributing to the prediction of the respective class, e.g., DeepLift [60] or GradCAM [61]. In this case, we propose to convert the heatmaps into a binary mask using a threshold  $t_{\text{cam}}$ .

#### Generation of Boxes in CutMix

It is necessary to generate different boxes with various side

lengths and areas throughout the CutMix process. Thus, to meet the requirement of controlling the box sizes, the implementation of CutMix needs to incorporate an input of a minimal area  $A_{\min} > 0$  and a maximal area  $A_{\max} \geq A_{\min} > 0$  of the box, denoted as the box size range  $A_{\min} - A_{\max}$ . Thus, for a box  $R = (r_a, r_b, r_c, r_d)$  the points are required to fulfill the inequality:

$$A_{\min} \leq (r_c - r_a)(r_d - r_b) \leq A_{\max}. \quad (12)$$

We propose an algorithm for creating the points that satisfy (12). It operates batch-wise by creating coordinates  $(r_a, r_b, r_c, r_d)$  for  $N_R$  boxes, which is the number of boxes needed for the batch-wise application of CutMix. The first step is to sample a list of box coordinates  $\mathcal{B}$  uniformly from  $[0, H]_{\mathbb{N}} \times [0, W]_{\mathbb{N}}$ . Thus, it is iterated until  $N_R$  points satisfy (12). If there are less than  $N_R$  points, every pair of points violating the condition is re-sampled. The pseudo-code of the algorithm is presented in Algorithm 1.

---

**Algorithm 1** Creation of Boxes

---

**Require:**  $A_{\min} > 0$ ;  $A_{\max} \geq A_{\min} > 0$ ;  $N_R, H, W \in \mathbb{N}$ .

**Ensure:** List of  $N_R$  valid random boxes.

```

1: Initialize empty list of boxes  $\mathcal{B}$ 
2: while  $|\mathcal{B}| < N_R$  do
3:   Sample  $\bar{r}_a, \bar{r}_c$  uniformly from  $[0, H]_{\mathbb{N}}$ 
4:   Sample  $\bar{r}_b, \bar{r}_d$  uniformly from  $[0, W]_{\mathbb{N}}$ 
5:    $r_a = \min(\bar{r}_a, \bar{r}_c)$ ;  $r_c = \max(\bar{r}_a, \bar{r}_c)$ 
6:    $r_b = \min(\bar{r}_b, \bar{r}_d)$ ;  $r_d = \max(\bar{r}_b, \bar{r}_d)$ 
7:   Calculate area  $A = (r_c - r_a)(r_d - r_b)$ 
8:   if  $A_{\min} \leq A \leq A_{\max}$  then
9:     Append  $(r_a, r_b, r_c, r_d)$  to  $\mathcal{B}$ 
10:  end if
11: end while
12: return  $\mathcal{B}$ 

```

---

*Multi-Label Scene Classification with CutMix and the proposed Label Propagation Strategy*

In the training phase of a deep neural network  $h$ , CutMix is applied to the selected images with a probability  $p$ . In each training step, after loading a batch from  $\mathcal{D}$ , random images  $\mathbf{x}_1$  and  $\mathbf{x}_2$  with their respective multi-label vectors  $\mathbf{y}_1$  and  $\mathbf{y}_2$  and reference maps  $\mathbf{m}_1$  and  $\mathbf{m}_2$  (or class explanation masks  $\mathbf{e}_1$  and  $\mathbf{e}_2$ ) are selected for the LP strategy enhanced augmentation process. The process yields a replacement of  $\mathbf{x}_1$  and  $\mathbf{y}_1$  by probability  $p$  with the augmented image  $\tilde{\mathbf{x}}$  and its updated multi-label vector  $\tilde{\mathbf{y}}$  that is derived by our LP strategy based on a pairing operation of the reference maps. It is worth noting that the one-to-one replacement ensures that the batch size is persistent. After training the deep neural network  $h$  with CutMix-augmented images together with our proposed LP strategy, the predicted multi-labels are assigned to images in the considered archive.

#### IV. DATASET DESCRIPTION AND EXPERIMENTAL DESIGN

In the experiments, we have used three RS multi-label datasets: 1) DeepGlobe-ML, which is a multi-label dataset that we constructed from the DeepGlobe Land Cover Classification

Challenge dataset [12], 2) BigEarthNet-S2 [18], and 3) TreeSatAI [62]. For each dataset, example images are shown in Figure 2. A comparison of the main characteristics of the considered datasets is provided in Table I, while the datasets are briefly described in the following.

##### A. Datasets

1) *DeepGlobe-ML*: The original DeepGlobe Land Cover Classification Challenge dataset [12] is collected from the DigitalGlobe +Vivid Images dataset that contains 1949 RGB tiles of size  $2448 \times 2448$  pixels with a spatial resolution of 0.5 m acquired over Thailand, Indonesia, and India. Each tile is associated with a manually annotated ground reference map. The classes comprise urban, agriculture, rangeland, forest, water, barren, and unknown. To ensure one MLC dataset associated with reliable reference maps in this paper, we constructed the DeepGlobe-ML from the original pixel-level classification dataset. To this end, all tiles were divided into a grid of  $120 \times 120$ -pixel patches. The respective multi-labels were then derived from the label information of the associated  $120 \times 120$ -pixel reference maps. We discarded all patches containing the class unknown. To account for an appropriate MLC dataset, we considered only 20% of the patches with a single present class and all patches with more than one present class, resulting in an average of 1.71 present classes per patch (cf., 1.28 present classes without discarding patches). In total, DeepGlobe-ML includes 30,443 patches and is split into a training set (60%), a validation set (20%), and a test set (20%).

2) *BigEarthNet-S2*: BigEarthNet-S2 [18] is a multi-label dataset that includes 590,326 Sentinel-2 multispectral images acquired over ten countries in Europe. The LULC class annotations are obtained from reference maps that originate from the publicly available thematic product CORINE Land Cover Map inventory of 2018 [15]. Following the LULC class nomenclature proposed in [63], each image is annotated with a subset of 19 LULC classes, including different types of forests, water, or complex urban or agricultural classes. The dataset contains an average of 2.95 present classes per image. In the experiments, a filtered subset that excludes patches with seasonal snow, clouds, and cloud shadows is used. The selected subset is divided into a training set (50%), a validation set (25%), and a test set (25%). Furthermore, only 10 bands (out of the originally 13 bands) with a spatial resolution of 10 m ( $120 \times 120$ -pixel) and 20 m ( $60 \times 60$ -pixel) are considered. It is worth noting that a preliminary version of the currently ongoing label update is used in our experiments.

3) *TreeSatAI*: The TreeSatAI dataset [62] is a multi-label tree species classification benchmark dataset that consists of 50,381 image-triplets of a high-resolution aerial image, a Sentinel-1 SAR and a Sentinel-2 multispectral image acquired over the German federal state of Lower Saxony. In our experiments, we only use the aerial images. Each of the  $304 \times 304$ -pixel aerial images includes the RGB and a near-infrared band with a spatial resolution of 0.5 m and is associated with multi-labels representing different species of trees from 15 genus



Figure 2: Example images of the datasets: (a) DeepGlobe-ML, (b) BigEarthNet-S2, and (c) TreeSatAI.

Table I: Characteristics of the multi-label scene classification datasets used in our experiments.

| Dataset             | $ \mathcal{D} $ | $L$ | Avg. $L$<br>per Image | $C$ | Image Sizes (Spatial Resolution) | Pixel-Level Reference Maps |
|---------------------|-----------------|-----|-----------------------|-----|----------------------------------|----------------------------|
| DeepGlobe-ML        | 18,185          | 6   | 1.71                  | 3   | 120×120 (0.5m)                   | Manually Annotated         |
| BigEarthNet-S2 [18] | 250,249         | 19  | 2.95                  | 10  | 120×120 (10m), 60×60 (20m)       | Thematic Product           |
| TreeSatAI [62]      | 40,332          | 15  | 1.59                  | 4   | 304×304 (0.2m)                   | Not available              |

classes. The labels were derived from forest administration data of the federal state of Lower Saxony that was annotated in the field or by photo interpretation. For the experiments, we chose a threshold of 5 % coverage of the pixels for a class to be annotated as present in the image. Further, we updated the original train-test split by also considering a validation set, yielding a training set of 80 %, a validation set of 10 %, and a test set of 10 % of the images. On average, there are 1.59 different tree species present in each image. It is worth noting that there exist no further pixel-level reference maps associated with this dataset. The application of our LP strategy is only possible when leveraging explanation methods (i.e., generating class explanation masks).

### B. Experimental Setup

For all our experiments, we use a randomly initialized ResNet18 from the `pytorch-image-models` library [64]. We choose a batch size of 300 and the cosine annealing learning rate scheduling with a start rate set to  $5e-4$  and warm-up iterations based on the number of steps. Each model is trained for 120 epochs. For reproducibility reasons, the global random state is fixed to seeds in the range of 42 to 46 implemented by the `seed-everything` functionality in `PyTorch lightning` [65]. We conduct every experiment with these five seeds and report the average of the test set performance in mean average precision macro (denoted as `mAP macro`) of the best model determined by the validation set. All experiments are carried out on an A100 SXM4 80GB GPU.

## V. EXPERIMENTAL RESULTS

The experimental results are organized as follows. In Section V-A, we assess the effectiveness of our LP strategy for

CutMix in RS MLC when reliable pixel-level reference maps are available. Subsequently, in Section V-B, we conduct an extensive ablation study on the effect of noisy reference maps on our LP strategy. To this end, we define and simulate noise types that can be related to different types of labeling errors. To further show the benefits in real use-cases beyond simulated noisy reference maps, in Section V-C, we study the effects of our LP strategy in a scenario in which the class positional information is extracted from noisy pixel-level reference maps derived from a thematic product. In Section V-D, we show the advantage of our LP strategy in a scenario in which we do not have access to reference maps and instead leverage the class positional information provided by an explanation method. Finally, in Section V-E we compare the effectiveness of CutMix with our LP strategy to other data augmentation techniques.

### A. Label Propagation based on Reliable Reference Maps

To evaluate the potential of leveraging pixel-level reference maps to correctly update the multi-labels during the application of CutMix in RS MLC, we initially study the effects of our proposed LP strategy when reliable reference maps are available. To this end, we report the results on the DeepGlobe-ML dataset. Therefore, we compare three different box augmentation techniques: i) CutOut; ii) CutMix without our proposed LP strategy, denoted as CutMix w/o LP; and CutMix with our proposed LP strategy, denoted as CutMix w LP<sub>map</sub>. As these techniques may favor different sizes of boxes, we conduct experiments for the value of the box size range  $A_{min} - A_{max}$  as 0.1–0.3, 0.1–0.5, 0.1–0.7, 0.3–0.5, and 0.3–0.7. All techniques are applied with a probability  $p$  of 0.5. The results are shown in Table II. It can be noted that our proposed LP strategy is effective under all tested box sizes. In addition, for each box size, it improves an application of CutMix without LP. In

particular, it can be observed that the larger the selected box sizes become, the more beneficial it is to apply our LP strategy. While for the box size range of 0.3–0.7 CutMix w LP<sub>map</sub> results in the best overall performance of all methods with 82.30 % in mAP macro, the box size range also yields one of the largest improvements to CutMix w/o LP. This improvement can be attributed to the highest probability of deleting class labels from one of the paired images. Further, in contrast to both CutMix techniques, it is worth noting that the performance of CutOut is more or less constant (i.e., invariant) for all evaluated box sizes except for very small box sizes (i.e., 0.1–0.3).

Table II: Results in mAP macro (%) for DeepGlobe-ML with associated reliable reference maps.

| CutMix Augmentation        |                |              |              |              |              |
|----------------------------|----------------|--------------|--------------|--------------|--------------|
| Method                     | Box Size Range |              |              |              |              |
|                            | 0.1–0.3        | 0.1–0.5      | 0.1–0.7      | 0.3–0.5      | 0.3–0.7      |
| CutMix w/o LP              | 78.93          | 79.17        | 79.76        | 80.25        | 80.49        |
| CutMix w LP <sub>map</sub> | <b>80.33</b>   | <b>80.74</b> | <b>80.72</b> | <b>82.21</b> | <b>82.30</b> |
| CutMix w LP <sub>xAI</sub> | <b>79.54</b>   | <b>79.70</b> | <b>80.24</b> | <b>81.96</b> | <b>82.01</b> |
| No Augmentation            |                |              |              |              |              |
| Baseline                   | 78.40          |              |              |              |              |

### B. Label Propagation based on Simulated Noisy Reference Maps

Only in rare cases there exist reliable pixel-level reference maps. In many scenarios, multi-labels are based on not fully reliable reference maps, and sometimes, even the estimation of class positional information via explanation methods is necessary. To better understand the effectiveness of our LP strategy, we conduct an extensive ablation study for six different types of noise in reference maps that simulate real scenarios. To this end, we define the following noise types: (i) Mask Shift, (ii) Dilation/Erosion, (iii) Rectify Borders, (iv) Border Deformation, (v) Segment Swap, and (vi) Class Swap. These noise types are studied to show the generalizability of our LP strategy to any arbitrary source of noisy class positional information. In the following, we illustrate intuitive examples per noise type. Nonetheless, many of the noise types can be associated with various scenarios. An illustration of the different noise types is shown in Figure 3. The example image is depicted in Figure 3a and the associated reference map in Figure 3b.

*Mask Shift.* Mask Shift is associated with an imperfect alignment of the reference map with the considered image (see Figure 3c). The most prominent example relates to an imprecise co-registration of image and label source if the class positional information is derived from a thematic product. To simulate this noise type, for a fraction  $f$  (in %) of reference maps associated with the training images, we apply a shift in a uniformly sampled direction with a uniformly sampled pixel shift taken from the interval of 0 and a maximum pixel shift  $\alpha_{\text{pixel\_shift}}$ .

*Dilation/Erosion.* Dilation/Erosion is associated with an inaccurate border of one consecutive class segment (i.e., an area that covers an individual class) that is proportionally enlarged or downsized (see Figure 3d). The most prominent example relates to the temporal difference between the image and label source if the class positional information is derived from a thematic product, e.g., a partially dried-out lake or a burned forest. To simulate this noise type, for a fraction  $f$  (in %) of reference maps associated with the training images, we uniformly select one class segment and either dilate or erode the segment for  $\alpha_{\text{iterations}}$  iterations.

*Rectify Borders.* Rectify Borders simulates pixel-level reference maps that are highly coarse (see Figure 3e). The most prominent example relates to different resolutions of image and label source if the class positional information is derived from a thematic product. To simulate this noise type, for a fraction  $f$  (in %) of reference maps associated with the training images, we first downsample its resolution by a magnitude of  $\alpha_{\text{magnitude}}$  and then resize it back to its original resolution.

*Border Deformation.* Border Deformation is associated with inaccurate borders between class segments of the reference map (see Figure 3f). The most prominent examples relate to (i) human annotation errors in the thematic product or the pixel-wise annotation of the considered image, (ii) inaccurate predictions of class segments if the class positional information is derived from the inference of a segmentation model (i.e., pixel-based classification model), or (iii) temporal differences between the considered image and thematic product, e.g., an urban area that was extended by a few buildings. To simulate this noise type, for a fraction  $f$  (in %) of reference maps associated with the training images, we place  $\alpha_{\text{max\_def}}$  small bounding boxes of varying size onto each reference map. If a bounding box overlays the border between two or more class segments, the whole bounding box gets assigned to one of the bordering classes selected at random. Otherwise, the bounding box gets assigned to the class it overlays (i.e., no alteration to the reference map is applied).

*Segment Swap.* Segment Swap is associated with an inaccurate positional assignment of a class (see Figure 3g). The most prominent example relates to a case in which the multi-labels are not associated with any reference maps and explanation methods are employed to estimate the class positional information, e.g., the class explanation masks associate the wrong parts of the image with a specific present class. To simulate this noise type, for a fraction  $f$  (in %) of reference maps associated with the training images, we remove one class segment and randomly place it in an aleatory polygon shape at a different location in the same reference map.

*Class Swap.* Class Swap is associated with inaccurate class assignments to class segments (see Figure 3h). The most prominent example relates to human annotation errors in the thematic product or in the pixel-wise annotation of the considered image, e.g., an ambiguous class is confused by the annotator. Another example relates to the incorrect prediction of class segments if the class positional information is derived from the inference of a segmentation model (i.e., pixel-based

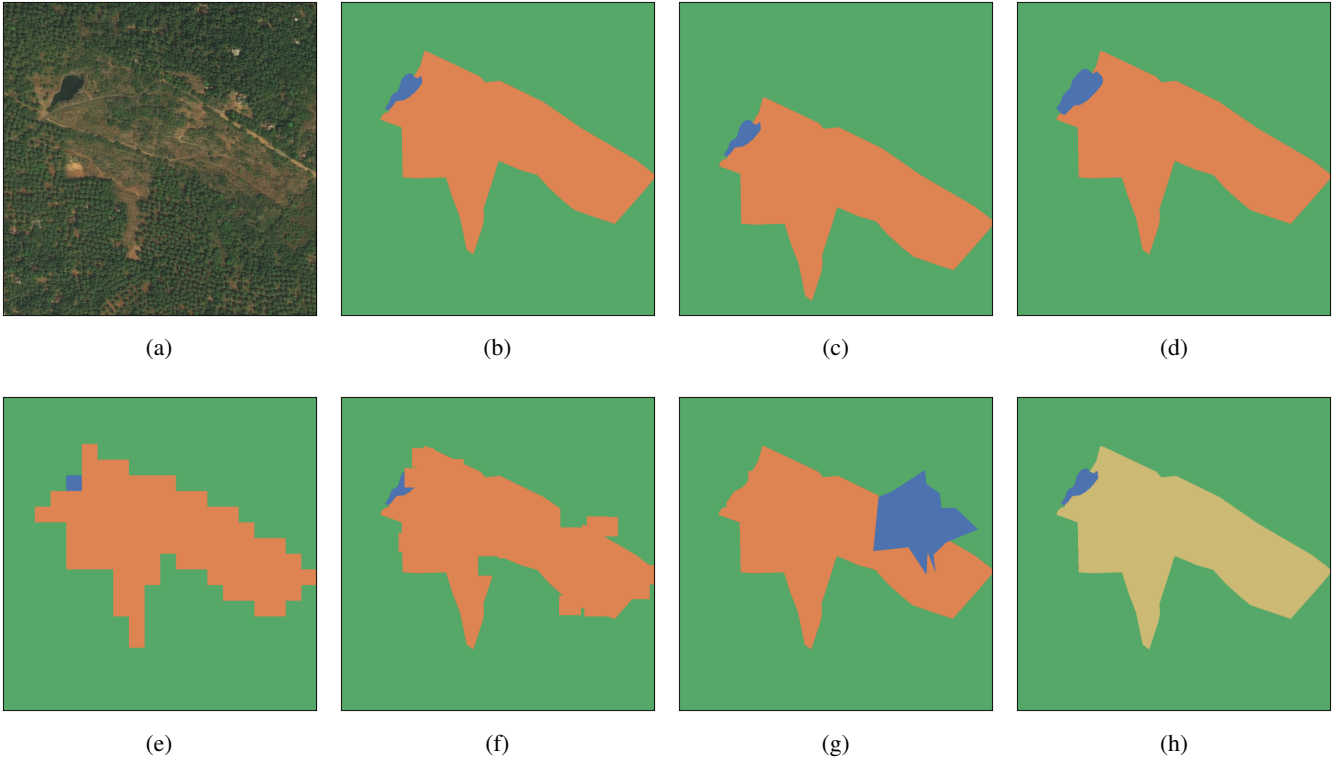


Figure 3: Examples of simulated noise in pixel-level reference maps: (a) original image, (b) original reference map, (c) Mask Shift, (d) Dilation/Erosion, (e) Rectify Borders, (f) Border Deformation, (g) Segment Swap, and (h) Class Swap.

classification model). To simulate this noise type, we assign a uniformly sampled new class for a fraction  $f$  (in %) of all class segments contained in all reference maps of the training set. It is worth noting that this noise type leads to multi-label noise. Thus, in this setting, we also update all multi-labels that are associated with noisy reference maps when comparing the performance of CutMix with and without our LP strategy.

Figure 4 shows the results associated with different types of noise in the reference maps for the DeepGlobe-ML dataset. All our experiments for CutMix w LP<sub>map</sub> are carried out with the best box size range of 0.3–0.7 and applied with a probability  $p$  of 0.5. The results are compared to CutMix w/o LP for the same box size range (see Section V-A). For Mask Shift, Dilation/Erosion, Rectify Border, and Border Deformation we applied the noise with varying intensity to different fractions of the reference maps (25 %, 50 %, 100 %). For Mask Shift, in all the considered settings, our proposed LP strategy yields better performance than CutMix without LP (see Figure 4a). While a maximum shift of 12 and 24 pixels (10 % and 20 % of the height) barely impacts model performance under any fraction of affected reference maps, only a strong noise induction of a maximum pixel shift of 36 (30 % of the height) has an observable negative impact on the overall performance if at least half of the reference maps are affected. Nonetheless, in comparison to the same setup without simulated noise (for same box size range, see Table II) it still results in a performance that is 1.5 % better in mAP macro. In contrast, the dilation or erosion of class segments significantly decreases the CutMix w LP<sub>map</sub> performance already at lighter intensities

(see Figure 4b). We observe a linear decrease in performance for the parameter of the fraction of reference maps as well as the iterations of applying dilation/erosion to a class segment, leading to the lowest mAP macro performance of 80.75 % for  $\alpha_{\text{iteration}}$  of 36 iterations. This setting yields similar performance to CutMix w/o LP, while our LP strategy yields better results under any other setting. A similar linear trend can be observed for noise in the form of a different resolution of reference maps than the images (see Figure 4c). However, its negative impact is less significant than Dilation/Erosion and the performance decrease is only minor. Under all tested settings, our LP strategy leads to higher performance than CutMix w/o LP. On the other hand, border deformations (see Figure 4d) do not seem to have an impact on model performance at all. While the performances of different parameter settings follow no clear pattern, none of them yields a deviation from the results under reliable reference maps of more than 0.2 % in mAP macro. This can be explained by the preservation of a high intersection over union between the reliable and the noisy reference maps as only the border regions are alternated. When entire class segments are moved to different areas in the reference map in a distinct shape, a linear trend can be observed between the fraction of segments moved and the performance of the model (see Figure 4e). Nevertheless, even for 30 % of the reference maps affected by segment swaps, leveraging our proposed LP strategy still improves CutMix w/o LP by about 1.5 % in mAP macro. For Class Swap, as changing the annotated class for segments leads to multi-label noise, each of the box size range settings for CutMix w/o LP had to be retrained. In line with the results without noise, for all three tested fractions of swapped class



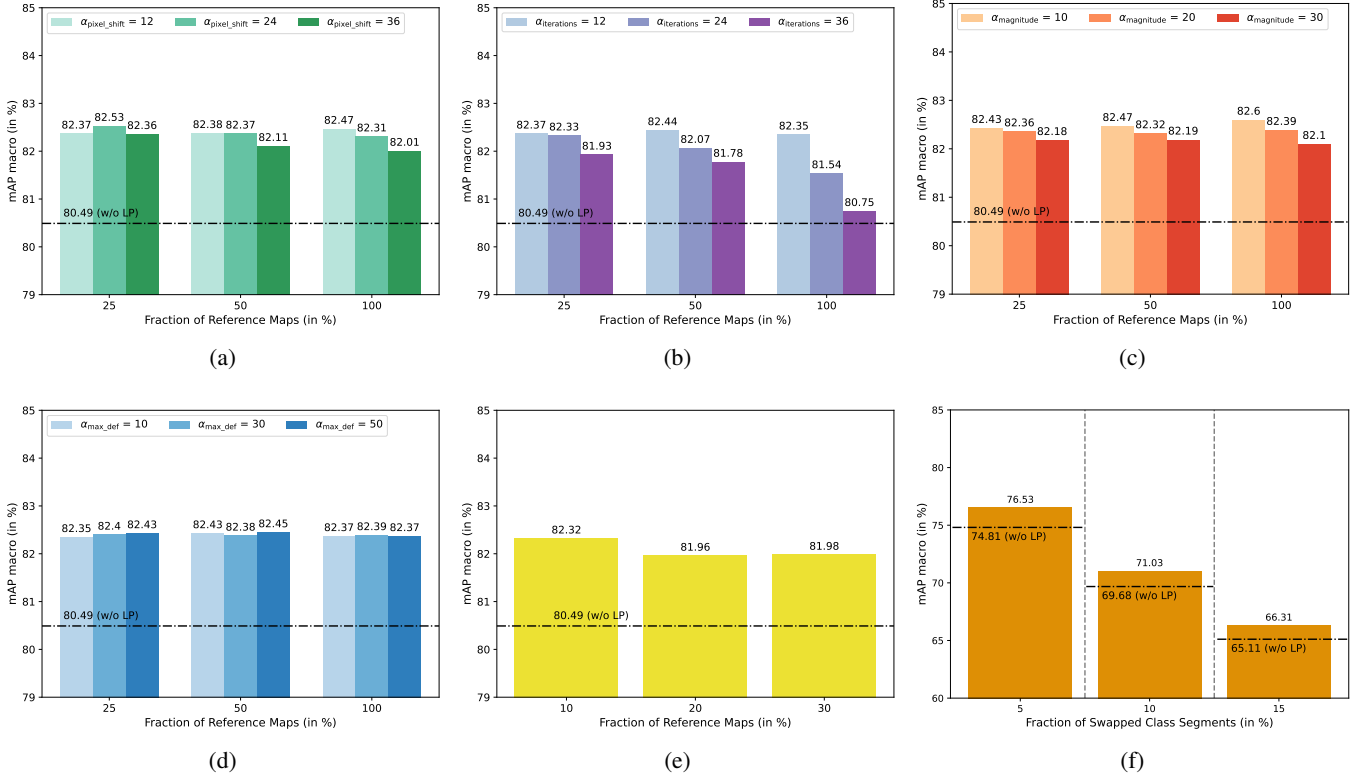


Figure 4: Results of simulated noise in pixel-level reference maps for DeepGlobe-ML: (a) Mask Shift, (b) Dilation/Erosion, (c) Rectify Borders, (d) Border Deformation, (e) Segment Swap, (f) Class Swap.

segments, the improvement of employing CutMix with our proposed LP strategy stays constant at around 1.5% in mAP macro (see Figure 4f). Under incorrectly annotated classes, the application of CutMix with our proposed LP strategy remains more effective than without it.

In summary, it was observed that inaccurate borders due to border deformation as well as annotation errors in terms of swapped class segments, do not impact the effectiveness of our proposed LP strategy at all. On the other hand, our experiments revealed some sensitivity to the shift of reference maps, low-resolution reference maps, the dilation/erosion, and the replacement of individual class segments. In particular, strong dilation or erosion of class segments that affect more than 50% of the reference maps may lead to similar performance to CutMix w/o LP when our LP strategy is employed. However, in all other tested settings, the decrease in performance due to noisy reference maps is not substantial. Thus, it is still beneficial to employ our proposed LP strategy over CutMix without a proper label update for all simulated noise types. This is due to the fact that the robustness of our LP strategy to noisy class positional information can be attributed to the fact that rough estimates are sufficient to correctly update the multi-labels. If a class covers a larger area in one of the remaining parts of the paired images, a single correctly annotated pixel in the reference map is enough to effectively update the multi-label of the augmented image using our LP strategy. The results indicate that the cases of wrong updates are less significant than the loss in information when our LP strategy is not used.

### C. Label Propagation based on Noisy Reference Maps from Thematic Products

To evaluate the effectiveness of our LP strategy in a scenario in which class positional information is provided in the form of a thematic product, we adopt the same setup from Section V-A for the BigEarthNet-S2 dataset. In line with the findings of our ablation study on simulated noisy reference maps, the usage of our LP strategy results in an improvement over CutMix without an effective label update (see Table III). Under all box size ranges tested, CutMix w  $\text{LP}_{\text{map}}$  consistently outperforms CutMix w/o LP. It is worth noting that the largest improvements are similar to those obtained for DeepGlobe-ML (see V-A) (about 2.0% in mAP macro) even though the class positional information contains more noise due to the usage of reference maps derived from a thematic product. The noisy class positional information originating from a thematic product does not impact the effectiveness of our LP strategy. Further, unlike DeepGlobe-ML, the box size range does not seem to play an important role in the generalization performance. CutMix w  $\text{LP}_{\text{map}}$  achieves the best results of about 76.7% in mAP macro for the box size ranges 0.1–0.3, 0.3–0.5, and 0.3–0.7; a clear trend in the reliance on smaller or larger boxes cannot be observed.

### D. Label Propagation based on Class Explanation Masks

Finally, to show the generalization capability of our proposed LP strategy to scenarios in which no associated pixel-level reference maps are available, we conduct experiments on TreeSatAI

Table III: Results in mAP macro (%) for BigEarthnet-S2 with associated noisy reference maps derived from a thematic product.

| CutMix Augmentation        |                |              |              |              |              |
|----------------------------|----------------|--------------|--------------|--------------|--------------|
| Method                     | Box Size Range |              |              |              |              |
|                            | 0.1–0.3        | 0.1–0.5      | 0.1–0.7      | 0.3–0.5      | 0.3–0.7      |
| CutMix w/o LP              | 75.42          | 74.90        | 74.69        | 74.52        | 75.39        |
| CutMix w LP <sub>map</sub> | <b>76.72</b>   | <b>76.32</b> | <b>76.05</b> | <b>76.76</b> | <b>76.72</b> |
| CutMix w LP <sub>xAI</sub> | <b>77.21</b>   | <b>77.22</b> | <b>77.21</b> | <b>78.26</b> | <b>78.43</b> |
| No Augmentation            |                |              |              |              |              |
| Baseline                   | 71.46          |              |              |              |              |

as well as on the DeepGlobe-ML and the BigEarthNet-S2 datasets assuming the unavailability of their reference maps. In this experiment, we apply the LP strategy to class explanation masks derived from an explanation method. To this end, we initially obtain the attribution of pixel importance from CAMs generated by the method Grad-CAM [61]. However, any other post hoc explanation method that is able to attribute multiple labels with the input pixels can be used. In this scenario, the workflow consists of two stages. First, a deep neural network is pre-trained on the task at hand until convergence without applying any augmentations. Then, a post hoc explanation method is applied to the pre-trained neural network to obtain the class explanation masks for each image. Thereafter, the actual training procedure that applies CutMix with our proposed LP strategy starts with a new training procedure from scratch. As CAMs comprise heatmaps with continuous values, a threshold is applied to obtain binary masks that fulfill the requirements defined in Section III-B to be leveraged by our LP strategy. For all experiments, we set the threshold  $t_{cam}$  as 0.1, while we set the second threshold for minimum activating pixels  $t_{map}$  as 10 to smooth uncertainty in border regions between activating and non-activating pixels. Nonetheless, it is worth noting that many parameter combinations for both threshold parameters can lead to reasonable performance. We applied a grid search that indicated almost neglectable differences. Three exemplary CAMs generated by GradCAM are shown in Figure 5.

Regarding box sizes and application probability of the investigated box augmentation techniques, we followed the same setup as previous experiments. From Table IV it can be observed that the results of TreeSatAI exhibit similar trends as with reliable reference maps. Even though TreeSatAI is the most challenging dataset and the class positional information is derived from noisy CAMs, the observations from reliable reference maps can be generalized to scenarios in which no associated reference maps are available. In line with the results of V-B, not fully reliable class positional information provided by explanation methods does not reduce the effectiveness of our proposed LP strategy. For all box size ranges tested, CutMix w LP<sub>xAI</sub> outperforms its counterpart without LP. Similarly, as observed for reliable reference maps, the more larger boxes are used, the better CutMix w LP<sub>xAI</sub> becomes, leading to the best mAP macro

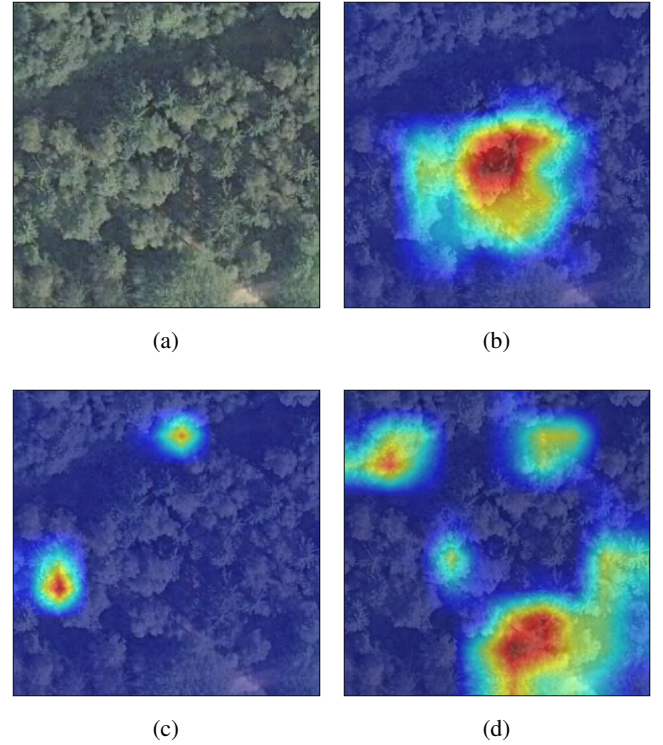


Figure 5: Examples for CAMs generated by Grad-CAM for TreeSatAI: (a) original image, (b) activation map for class Betula, (c) activation map for class Pinus, and (d) activation map for class Quercus.

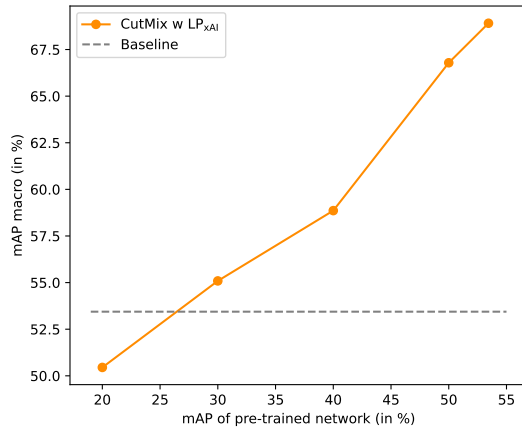
of 68.91 % for a box size range of 0.3–0.7. The effectiveness of using LP strategy based on class explanation masks is also observable for DeepGlobe-ML and BigEarthNet-S2 (see CutMix w LP<sub>xAI</sub> in Table II and Table III) respectively. It is noteworthy that class explanation masks yield almost on-par results with reliable reference maps and better results than not fully reliable reference maps. Furthermore, an ablation study comparing class explanation masks derived from pre-trained networks with varying levels of performance shows that our LP strategy based on class explanation masks is already effective when the class explanation masks are obtained from pre-trained models that are less performant. Figure 6 shows the results of the LP strategy based on class explanation masks obtained from intermediate model states saved during pre-training (stage one) on TreeSatAI with a fixed box size range of 0.3–0.7. It can be seen that already at a pre-training mAP macro of 30 % the produced explanation masks provide enough reliable class positional information such that CutMix w LP<sub>xAI</sub> outperforms the baseline without augmentation. Consequently, our LP strategy demonstrates effectiveness also for scenarios in which explanation methods are leveraged to obtain class positional information to allow the effective use of CutMix in MLC.

#### E. Comparison with other Data Augmentation Techniques

To contextualize the effectiveness of our proposed LP strategy within the broader landscape of other data augmentation techniques, we compare its performance against standard augmentation methods, including CutOut, Random Resize

Table IV: Results in mAP macro (%) for TreesSatAI with associated class explanation masks obtained by the thresholded CAMs.

| CutMix Augmentation        |                |              |              |              |              |
|----------------------------|----------------|--------------|--------------|--------------|--------------|
| Method                     | Box Size Range |              |              |              |              |
|                            | 0.1–0.3        | 0.1–0.5      | 0.1–0.7      | 0.3–0.5      | 0.3–0.7      |
| CutMix w/o LP              | 57.42          | 58.78        | 60.19        | 63.82        | 64.67        |
| CutMix w LP <sub>xAI</sub> | <b>62.04</b>   | <b>63.51</b> | <b>64.48</b> | <b>68.77</b> | <b>68.91</b> |
| No Augmentation            |                |              |              |              |              |
| Baseline                   | 53.44          |              |              |              |              |

Figure 6: Ablation study on using pre-trained networks of varying levels of performance to generate class explanation masks for the CutMix w LP<sub>xAI</sub> training on TreeSatAI.

Crop, and Random Rotate. The results of these comparisons on the DeepGlobe-ML dataset are presented in Table V. The baseline model, trained without any augmentation, achieves an AP macro of 78.40%. Among the conventional augmentation techniques, Random Resize Crop provides the highest improvement, yielding an AP macro of 81.41%. When examining the impact of CutMix, we observe a notable performance boost. Without our LP strategy, CutMix achieves an AP macro of 80.49%, already surpassing CutOut and Random Rotate. However, when incorporating our LP strategy, the improvements become even more pronounced. CutMix w LP<sub>map</sub> achieves the best overall performance, reaching 82.30% in AP macro, outperforming all other augmentation strategies. Similarly, CutMix w LP<sub>xAI</sub> achieves an AP macro of 82.01%, demonstrating the effectiveness of leveraging class positional information derived from explanation methods. These results confirm that the proposed LP strategy not only enhances the effectiveness of CutMix but also outperforms commonly used geometric augmentation techniques. The significant improvements in AP macro underscore the importance of accurate multi-label propagation in MLC, particularly when class positional information is available. Moreover, the gains observed with CutMix w LP<sub>xAI</sub> highlight the feasibility of employing explanation-driven class positional information in cases where explicit reference maps are unavailable.

Table V: Comparison of CutMix using our proposed LP strategy with other geometric data augmentation techniques for DeepGlobe-ML.

| Method                     | mAP macro    | mAP micro    |
|----------------------------|--------------|--------------|
| Baseline                   | 78.40        | 82.90        |
| CutOut                     | 79.69        | 84.93        |
| RandomResizeCrop           | 81.41        | 86.72        |
| RandomRotate               | 78.55        | 83.75        |
| CutMix w/o LP              | 80.49        | 83.65        |
| CutMix w LP <sub>map</sub> | <b>82.30</b> | <b>87.25</b> |
| CutMix w LP <sub>xAI</sub> | 82.01        | 86.88        |

## VI. CONCLUSION

In this article, we have proposed a label propagation (LP) strategy that allows the effective application of CutMix in the framework of multi-label image classification (MLC) in remote sensing (RS). The direct application of CutMix to training images annotated with multi-labels can lead to the potential erasure or addition of class labels in the paired image and, thus, may lead to multi-label noise. The proposed LP strategy overcomes this problem by preserving the correct class information within the multi-label vector of the augmented image to enable an effective application of CutMix in MLC. In detail, it exploits pixel-level class positional information such that the preservation of the correct multi-labels of erased and copied areas can be guaranteed. The pixel-level class positional information can either originate from associated pixel-level reference maps or class explanation masks generated by explanation methods. Similarly to the pairing operation of CutMix for two images, our proposed LP strategy pairs the associated pixel-level class positional information from both images to derive the updated multi-label vector for the augmented image. The results show the effectiveness of the LP strategy under reliable associated reference maps and under various simulated noisy reference maps with less reliable class positional information. In line with the observations from the simulated noisy reference maps, our proposed LP strategy proves to be effective in real scenarios when leveraging noisy reference maps derived from thematic products, as well as integrating class explanation masks when no associated reference maps are available. The reason for the robustness of our LP strategy under not fully accurate class positional information is that for assigning high-level categories in an MLC task rough estimates of class positional information can be sufficient to update the multi-label vector of the augmented image. Consequently, integrating our proposed LP strategy allows the application of CutMix in RS MLC without being affected by multi-label noise.

As a final remark, we would like to note that the proposed strategy is promising for possible operational applications in which associated class positional information might not be fully reliable due to both its general properties and its simplicity in the implementation. However, label imbalances can affect the performance in MLC tasks, particularly for underrepresented classes. The CutMix algorithm with our LP strategy does not change the expected label distribution. As a future work,



we plan to adapt CutMix to account for label imbalances in multi-label training sets to further improve the generalization capabilities of deep neural networks trained on multi-label RS image classification tasks.

## VII. ACKNOWLEDGEMENT

This work is supported by the European Research Council (ERC) through the ERC-2017-STG BigEarth Project under Grant 759764.

## REFERENCES

- [1] G. Sumbul and B. Demir, "A deep multi-attention driven approach for multi-label remote sensing image classification," in *IEEE Access*, vol. 8, pp. 95934–95946, 2020.
- [2] Y. Li, R. Chen, Y. Zhang, M. Zhang, and L. Chen, "Multi-label remote sensing image scene classification by combining a convolutional neural network and a graph neural network," in *Remote Sensing*, vol. 23, p. 4003, 12, 2020.
- [3] H. Yessou, G. Sumbul, and B. Demir, "A comparative study of deep learning loss functions for multi-label remote sensing image classification," in *IEEE International Geoscience and Remote Sensing Symposium*, pp. 1349–1352, 2020.
- [4] R. Stivaktakis, G. Tsagkatakis, and P. Tsakalides, "Deep learning for multilabel land cover scene categorization using data augmentation," *IEEE Geoscience and Remote Sensing Letters*, vol. 16, no. 7, pp. 1031–1035, 2019.
- [5] S. Yun, D. Han, S. J. Oh, S. Chun, J. Choe, and Y. Yoo, "CutMix: Regularization strategy to train strong classifiers with localizable features," in *Proceedings of the IEEE/CVF International Conference on Computer Vision*, pp. 6023–6032, 2019.
- [6] T. DeVries and G. W. Taylor, "Improved regularization of convolutional neural networks with cutout," in *arXiv preprint arXiv:1708.04552*, 2017.
- [7] Z. Zhong, L. Zheng, G. Kang, S. Li, and Y. Yang, "Random erasing data augmentation," in *Proceedings of the AAAI Conference on Artificial Intelligence*, vol. 34, pp. 13001–13008, 2020.
- [8] X. Lu, C. Zhang, Q. Ye, C. Wang, C. Yang, and Q. Wang, "RSI-Mix: Data augmentation method for remote sensing image classification," in *7th International Conference on Intelligent Computing and Signal Processing*, pp. 1982–1985, 2022.
- [9] Z. Suo, Y. Zhao, S. Chen, and Y. Hu, "BoxPaste: An effective data augmentation method for SAR ship detection," *Remote Sensing*, vol. 14, no. 22, 2022.
- [10] J.-X. Wang, S.-B. Chen, C. H. Q. Ding, J. Tang, and B. Luo, "RanPaste: Paste consistency and pseudo label for semisupervised remote sensing image semantic segmentation," *IEEE Transactions on Geoscience and Remote Sensing*, vol. 60, pp. 1–16, 2022.
- [11] T. Burgert, M. Ravanbakhsh, and B. Demir, "On the effects of different types of label noise in multi-label remote sensing image classification," *IEEE Transactions on Geoscience and Remote Sensing*, vol. 60, pp. 1–13, 2022.
- [12] I. Demir, K. Koperski, D. Lindenbaum, G. Pang, J. Huang, S. Basu, F. Hughes, D. Tuia, and R. Raskar, "Deepglobe 2018: A challenge to parse the earth through satellite images," in *Proceedings of the IEEE Conference on Computer Vision and Pattern Recognition Workshops*, pp. 172–181, 2018.
- [13] C. F. Brown, S. P. Brumby, B. Guzder-Williams, T. Birch, S. B. Hyde, J. Mazzariello, W. Czerwinski, V. J. Pasquarella, R. Haertel, S. Ilyushchenko, K. Schwehr, M. Weisse, F. Stolle, C. Hanson, O. Guinan, R. Moore, and A. M. Tait, "Dynamic World, Near real-time global 10 m land use land cover mapping," *Scientific Data*, vol. 9, no. 1, p. 251, 2022.
- [14] C. Paris and L. Bruzzone, "A novel approach to the unsupervised extraction of reliable training samples from thematic products," *IEEE Transactions on Geoscience and Remote Sensing*, vol. 59, no. 3, pp. 1930–1948, 2020.
- [15] G. Büttner, J. Feranec, G. Jaffrain, L. Mari, G. Maucha, and T. Soukup, "The CORINE land cover 2000 project," *EARSeL eProceedings*, vol. 3, no. 3, pp. 331–346, 2004.
- [16] O. Arino, J. J. R. Perez, V. Kalogirou, S. Bontemps, P. Defourny, and E. V. Bogaert, "Global land cover map for 2009 (GlobCover 2009)," 2012.
- [17] E. Bartholomé, A. Belward, A. Frédéric, S. Bartalev, C. Carmona-Moreno, H. Eva, S. Fritz, J. Grégoire, P. Mayaux, and H.-J. Stibig, *GLC 2000: Global land cover mapping for the year 2000*. 2002.
- [18] G. Sumbul, M. Charfuelan, B. Demir, and V. Markl, "Bigearthnet: A large-scale benchmark archive for remote sensing image understanding," in *IEEE International Geoscience and Remote Sensing Symposium*, pp. 5901–5904, 2019.
- [19] K. He, X. Zhang, S. Ren, and J. Sun, "Deep residual learning for image recognition," in *Proceedings of the IEEE Conference on Computer Vision and Pattern Recognition*, pp. 770–778, 2016.
- [20] M. Tan and Q. Le, "Efficientnet: Rethinking model scaling for convolutional neural networks," in *International Conference on Machine Learning*, pp. 6105–6114, 2019.
- [21] Z. Liu, H. Mao, C.-Y. Wu, C. Feichtenhofer, T. Darrell, and S. Xie, "A convnet for the 2020s," in *Proceedings of the IEEE/CVF Conference on Computer Vision and Pattern Recognition*, pp. 11976–11986, 2022.
- [22] Q. Xie, M.-T. Luong, E. Hovy, and Q. V. Le, "Self-training with noisy student improves imagenet classification," in *Proceedings of the IEEE/CVF Conference on Computer Vision and Pattern Recognition*, pp. 10687–10698, 2020.
- [23] D. Berthelot, N. Carlini, I. Goodfellow, N. Papernot, A. Oliver, and C. A. Raffel, "Mixmatch: A holistic approach to semi-supervised learning," *Advances in Neural Information Processing Systems*, vol. 32, 2019.
- [24] K. Sohn, D. Berthelot, N. Carlini, Z. Zhang, H. Zhang, C. A. Raffel, E. D. Cubuk, A. Kurakin, and C.-L. Li, "Fixmatch: Simplifying semi-supervised learning with consistency and confidence," *Advances in Neural Information Processing Systems*, vol. 33, pp. 596–608, 2020.
- [25] T. Chen, S. Kornblith, M. Norouzi, and G. Hinton, "A simple framework for contrastive learning of visual representations," in *Proceedings of the 37th International Conference on Machine Learning*, vol. 119, pp. 1597–1607, July 2020.
- [26] K. He, H. Fan, Y. Wu, S. Xie, and R. Girshick, "Momentum contrast for unsupervised visual representation learning," in *Proceedings of the IEEE/CVF Conference on Computer Vision and Pattern Recognition*, pp. 9729–9738, 2020.
- [27] M. Caron, H. Touvron, I. Misra, H. Jégou, J. Mairal, P. Bojanowski, and A. Joulin, "Emerging properties in self-supervised vision transformers," in *Proceedings of the IEEE/CVF International Conference on Computer Vision*, pp. 9650–9660, 2021.
- [28] A. Bochkovskiy, C.-Y. Wang, and H.-Y. M. Liao, "Yolov4: Optimal speed and accuracy of object detection," *arXiv preprint arXiv:2004.10934*, 2020.
- [29] G. Ghiasi, Y. Cui, A. Srinivas, R. Qian, T.-Y. Lin, E. D. Cubuk, Q. V. Le, and B. Zoph, "Simple copy-paste is a strong data augmentation method for instance segmentation," in *Proceedings of the IEEE/CVF Conference on Computer Vision and Pattern Recognition*, pp. 2918–2928, 2021.
- [30] J. Ding, B. Chen, H. Liu, and M. Huang, "Convolutional neural network with data augmentation for SAR target recognition," *IEEE Geoscience and Remote Sensing Letters*, vol. 13, no. 3, pp. 364–368, 2016.
- [31] P. Yan, F. He, Y. Yang, and F. Hu, "Semi-supervised representation learning for remote sensing image classification based on generative adversarial networks," *IEEE Access*, vol. 8, pp. 54135–54144, 2020.

- [32] Q. Xiao, B. Liu, Z. Li, W. Ni, Z. Yang, and L. Li, "Progressive data augmentation method for remote sensing ship image classification based on imaging simulation system and neural style transfer," *IEEE Journal of Selected Topics in Applied Earth Observations and Remote Sensing*, vol. 14, pp. 9176–9186, 2021.
- [33] W. Zhang and Y. Cao, "A new data augmentation method of remote sensing dataset based on Class Activation Map," *Journal of Physics: Conference Series*, vol. 1961, no. 1, p. 012023, 2021.
- [34] Y. Yan, Z. Tan, and N. Su, "A data augmentation strategy based on simulated samples for ship detection in RGB remote sensing images," *ISPRS International Journal of Geo-Information*, vol. 8, no. 6, 2019.
- [35] K. Zheng, M. Wei, G. Sun, B. Anas, and Y. Li, "Using vehicle synthesis generative adversarial networks to improve vehicle detection in remote sensing images," *ISPRS International Journal of Geo-Information*, vol. 8, no. 9, 2019.
- [36] Z. Zhang, Z. Feng, and S. Yang, "Semi-supervised object detection framework with object first mixup for remote sensing images," in *IEEE International Geoscience and Remote Sensing Symposium*, pp. 2596–2599, 2021.
- [37] B. Zhao, Y. Wu, X. Guan, L. Gao, and B. Zhang, "An improved aggregated-mosaic method for the sparse object detection of remote sensing imagery," *Remote Sensing*, vol. 13, no. 13, 2021.
- [38] G. Chen, G. Pei, Y. Tang, T. Chen, and Z. Tang, "A novel multi-sample data augmentation method for oriented object detection in remote sensing images," in *IEEE 24th International Workshop on Multimedia Signal Processing*, pp. 1–7, 2022.
- [39] Z.-H. You, J.-X. Wang, S.-B. Chen, J. Tang, and B. Luo, "FMWDCT: Foreground mixup into weighted dual-network cross training for semisupervised remote sensing road extraction," *IEEE Journal of Selected Topics in Applied Earth Observations and Remote Sensing*, vol. 15, pp. 5570–5579, 2022.
- [40] D. Ciregan, U. Meier, and J. Schmidhuber, "Multi-column deep neural networks for image classification," in *IEEE Conference on Computer Vision and Pattern Recognition*, pp. 3642–3649, 2012.
- [41] A. Krizhevsky, G. Hinton, and others, "Learning multiple layers of features from tiny images," 2009.
- [42] J. Deng, W. Dong, R. Socher, L.-J. Li, K. Li, and L. Fei-Fei, "Imagenet: A large-scale hierarchical image database," in *Proceedings of the IEEE Conference on Computer Vision and Pattern Recognition*, pp. 248–255, 2009.
- [43] A. Krizhevsky, I. Sutskever, and G. E. Hinton, "ImageNet classification with deep convolutional neural networks," in *Advances in Neural Information Processing Systems*, vol. 25, 2012.
- [44] S. Zagoruyko and N. Komodakis, "Wide residual networks," in *Proceedings of the British Machine Vision Conference*, pp. 87.1–87.12, 2016.
- [45] B. Zoph, V. Vasudevan, J. Shlens, and Q. V. Le, "Learning transferable architectures for scalable image recognition," in *Proceedings of the IEEE Conference on Computer Vision and Pattern Recognition*, pp. 8697–8710, 2018.
- [46] M. Neumann, A. S. Pinto, X. Zhai, and N. Houlsby, "In-domain representation learning for remote sensing," *arXiv preprint arXiv:1911.06721*, 2019.
- [47] Y. Bazi, L. Bashmal, M. M. A. Rahhal, R. A. Dayil, and N. A. Ajlan, "Vision transformers for remote sensing image classification," *Remote Sensing*, vol. 13, no. 3, 2021.
- [48] D. Wang, J. Zhang, B. Du, G.-S. Xia, and D. Tao, "An empirical study of remote sensing pretraining," *IEEE Transactions on Geoscience and Remote Sensing*, vol. 61, pp. 1–20, 2023.
- [49] M. Oquab, L. Bottou, I. Laptev, and J. Sivic, "Is object localization for free?-weakly-supervised learning with convolutional neural networks," in *Proceedings of the IEEE Conference on Computer Vision and Pattern Recognition*, pp. 685–694, 2015.
- [50] L. Sixt, B. Wild, and T. Landgraf, "RenderGAN: Generating realistic labeled data," *Frontiers in Robotics and AI*, vol. 5, 2018.
- [51] Q. Wu, Y. Chen, and J. Meng, "DCGAN-based data augmentation for tomato leaf disease identification," *IEEE Access*, vol. 8, pp. 98716–98728, 2020.
- [52] A. Antoniou, A. Storkey, and H. Edwards, "Data augmentation generative adversarial networks," in *International Conference on Learning Representations*, 2018.
- [53] R. Geirhos, P. Rubisch, C. Michaelis, M. Bethge, F. A. Wichmann, and W. Brendel, "ImageNet-trained CNNs are biased towards texture; increasing shape bias improves accuracy and robustness," in *International Conference on Learning Representations*, 2018.
- [54] Y. Yan, Y. Zhang, and N. Su, "A novel data augmentation method for detection of specific aircraft in remote sensing RGB images," *IEEE Access*, vol. 7, pp. 56051–56061, 2019.
- [55] H. Zhang, M. Cisse, Y. N. Dauphin, and D. Lopez-Paz, "Mixup: beyond empirical risk minimization," in *International Conference on Learning Representations*, 2018.
- [56] J. Li, R. Socher, and S. C. Hoi, "DivideMix: Learning with noisy labels as semi-supervised learning," in *International Conference on Learning Representations*, 2019.
- [57] D. Walawalkar, Z. Shen, Z. Liu, and M. Savvides, "Attentive Cutmix: An enhanced data augmentation approach for deep learning based image classification," in *IEEE International Conference on Acoustics, Speech and Signal Processing*, pp. 3642–3646, 2020.
- [58] D. Dwibedi, I. Misra, and M. Hebert, "Cut, paste and learn: Surprisingly easy synthesis for instance detection," in *Proceedings of the IEEE International Conference on Computer Vision*, pp. 1301–1310, 2017.
- [59] N. V. Chawla, K. W. Bowyer, L. O. Hall, and W. P. Kegelmeyer, "SMOTE: Synthetic minority over-sampling technique," *Journal of Artificial Intelligence Research*, vol. 16, no. 1, pp. 321–357, 2002.
- [60] A. Shrikumar, P. Greenside, and A. Kundaje, "Learning important features through propagating activation differences," in *International Conference on Machine Learning*, pp. 3145–3153, PMLR, 2017.
- [61] R. R. Selvaraju, M. Cogswell, A. Das, R. Vedantam, D. Parikh, and D. Batra, "Grad-cam: Visual explanations from deep networks via gradient-based localization," in *Proceedings of the IEEE International Conference on Computer Vision*, pp. 618–626, 2017.
- [62] S. Ahlswede, C. Schulz, C. Gava, P. Helber, B. Bischke, M. Förster, F. Arias, J. Hees, B. Demir, and B. Kleinschmit, "TreeSatAI benchmark archive: A multi-sensor, multi-label dataset for tree species classification in remote sensing," *Earth System Science Data Discussions*, vol. 2022, pp. 1–22, 2022.
- [63] G. Sumbul, A. de Wall, T. Kreuziger, F. Marcelino, H. Costa, P. Benevides, M. Caetano, B. Demir, and V. Markl, "BigEarthNet-MM: A large-scale, multimodal, multilabel benchmark archive for remote sensing image classification and retrieval [software and data sets]," *IEEE Geoscience and Remote Sensing Magazine*, vol. 9, no. 3, pp. 174–180, 2021.
- [64] R. Wightman, "PyTorch Image Models," 2019. Publication Title: GitHub repository.
- [65] W. Falcon and The PyTorch Lightning team, "PyTorch Lightning," Mar. 2019.